

Calibration harp

April 11, 2011

Abstract

Abstract

Plumb line lens distortion correction methods permit to avoid numerical compensation between the camera internal and external parameters in global calibration method. Once the distortion has been corrected by a plumb line method, the camera is ensured to transform, up to the distortion precision, 3D straight lines into 2D straight lines, and therefore becomes a pinhole camera. This paper introduces a plumb line method for correcting and evaluating camera lens distortion with high precision. The evaluation criterion is defined as the average standard deviation from straightness of a set of approximately equally spaced straight strings photographed uniformly in all directions by the camera, so that their image crosses the whole camera field. The method uses an easily built “calibration harp,” namely a frame on which good quality strings have been tightly stretched to ensure a very high physical straightness. Real experiments confirm that our method produces high precision corrections (less than 0.05 pixel), approximating the distortion with a large number of degrees of freedom given by a polynomial model of order eleven. This precision is again improved by a factor about 2 by using fishing strings which are more smooth.

1 Introduction

This paper presents a method to correct camera lens distortion with high precision. By high precision, we mean figures like a 0.1 pixel deviation from straightness for a straight line crossing the whole camera field. Such a precision is not necessary for the human vision which is not affected by distortions of less than 2 pixels. However, there is no limit to the desired precision when the camera is used for 3D reconstruction or photogrammetry tasks. Traditionally, lens distortion and the other camera parameters are estimated simultaneously as camera internal and external parameters [21, 23, 26, 16, 24]. In these global calibration methods all parameters are estimated by minimizing the error between the camera and its numerical model on feature points identified in several views, all in a single non-linear optimization. The result will be precise if (and only if) the model captures the correct physical property

of cameras and if the minimization algorithm finds a global minimum. Unfortunately global camera calibration suffers a common drawback: errors in the external and internal camera parameter can be compensated by opposite errors in the distortion model. Thus the residual error can be apparently small, while the distortion model is not precisely estimated [24, 17]. For example the Lavest *et al.* method [16] measures the non-flatness of a pattern and yields a remarkably small re-projection error of about 0.02 pixels, while the straightness of corrected lines has a 0.2 pixel RMSE. This drawback becomes more serious for high resolution camera because the same amount of camera orientation/position error can cause more error in pixels in image compared to low resolution camera ¹. This implies more freedom in the distortion model to compensate the error. The error compensation in global calibration can be avoided by proceeding to distortion correction before camera calibration. Recent distortion correction methods use the correspondences between two or several images, without knowledge of any camera information. The main tool they use is slackened epipolar constraints, which incorporate lens distortion into the epipolar geometry. Several iterative [22, 25] or non-iterative methods [4, 13, 5, 17, 8] are used to estimate the distortion and to correct it. These methods are used with a low order parametric distortion model and therefore cannot achieve high precision.

Non-parametric methods which establish a direct diffeomorphism between a flat pattern and a frontal photograph of it [14, 9] should be ideal for high precision distortion correction. Indeed, they do not depend on the *a priori* choice of a distortion model with a fixed number of parameters. Yet to achieve a high precision, they depend on the design of a very flat non deformable plate with highly accurate patterns printed on it². This replaces a technological challenge by another, which is not simpler. Plumb-line methods [6] should therefore be an alternative, provided it is easier to create very straight lines. For plumb-line methods, an appropriate distortion model still is necessary to precisely remove the distortion. Almost all of the existing models can be directly incorporated into a plumb-line method. But some of them are too complicated [6], while some are not general enough to capture the distortion [12]. For most distortion models, the distortion center is a sensitive parameter when a realistic distortion is treated. The bare polynomials proposed in [19] are therefore a good choice, being a translation invariant and linear approximation of any vector field. This model free approximation can approximate complex radial and non-radial distortions as well provided its degree is high enough. According to the criteria of *self-consistency* and *universality* ³ developed in [19] to compare many camera dis-

¹Assume a camera CCD covers a 60° field of view and has 0.1° orientation error. For a low resolution camera 512 × 512 pixels CCD, the 0.1° orientation error corresponds to 0.85 pixels in image, while for a high resolution camera with a 1280 × 1280 pixels CCD, the error becomes 2.13 pixels.

²10 micron flatness is needed to achieve the precision 0.01 pixels.

³Self-consistency is evaluated by the residual error when distortion generated with a certain model is corrected (using the model in reverse way) by the best parameters for the same model.

tortion models, the polynomial models are the most flexible and accurate.

The proposed method is introduced in section 2, followed by real experiments in section 3, along with a comparison to other methods. The error compensation in global camera calibration is shown in section ???. Section 6 is a conclusion.

2 The harp calibration method

In one sentence, the proposed method combines the advantage of plumb-line methods with the universality of the model free polynomial approximation. The plumb-line method consists in correcting the distorted points which are supposed to be on a straight line, by minimizing the average distance from the corrected points to their corresponding regression lines. In the sequel, denote (x_u, y_u) undistorted point, (x_d, y_d) distorted point, (x_c, y_c) distortion center, (\bar{x}_u, \bar{y}_u) radial undistorted point and (\bar{x}_d, \bar{y}_d) radial distorted point with $\bar{x}_u = x_u - x_c$, $\bar{y}_u = y_u - y_c$, $\bar{x}_d = x_d - x_c$ and $\bar{y}_d = y_d - y_c$. The distorted radius $r_d = \sqrt{\bar{x}_d^2 + \bar{y}_d^2}$ and the undistorted radius $r_u = \sqrt{\bar{x}_u^2 + \bar{y}_u^2}$.

2.1 Polynomial model

Unlike many radial symmetric distortion models, polynomial model is not radial symmetric and the distortion in x and y direction is modeled with different parameters and different order. Denote p and q the order of distortion for x and y component respectively, polynomial model has the following form:

$$\begin{aligned}
\bar{x}_d &= b_0 \bar{x}_u^p + b_1 \bar{x}_u^{p-1} \bar{y}_u + b_2 \bar{x}_u^{p-2} \bar{y}_u^2 + \cdots + b_p \bar{y}_u^p \\
&\quad + b_{p+1} \bar{x}_u^{p-1} + b_{p+2} \bar{x}_u^{p-2} \bar{y}_u + \cdots + b_{2p} \bar{y}_u^{p-1} \\
&\quad + \cdots + b_{\frac{(p+1)(p+2)}{2}-3} \bar{x}_u + b_{\frac{(p+1)(p+2)}{2}-2} \bar{y}_u \\
&\quad + b_{\frac{(p+1)(p+2)}{2}-1} \\
\bar{y}_d &= c_0 \bar{x}_u^q + c_1 \bar{x}_u^{q-1} \bar{y}_u + c_2 \bar{x}_u^{q-2} \bar{y}_u^2 + \cdots + c_q \bar{y}_u^q \\
&\quad + c_{q+1} \bar{x}_u^{q-1} + c_{q+2} \bar{x}_u^{q-2} \bar{y}_u + \cdots + c_{2q} \bar{y}_u^{q-1} \\
&\quad + \cdots + c_{\frac{(q+1)(q+2)}{2}-3} \bar{x}_u + c_{\frac{(q+1)(q+2)}{2}-2} \bar{y}_u \\
&\quad + c_{\frac{(q+1)(q+2)}{2}-1}.
\end{aligned} \tag{1}$$

The number of parameters for x and y component is respectively $\frac{(p+1)(p+2)}{2}$ and $\frac{(q+1)(q+2)}{2}$. The model is called bicubic model if $p = q = 3$. Note that the change of the distortion center (x_c, y_c) can be compensated by the parameters. So (x_c, y_c) can be arbitrarily set without changing the correction performance, which makes this model quite handy. By the analysis in [19], polynomial model is self-consistent and more universal

Analogously, universality is measured by the residual error when a model is used to correct distortions generated by a family of other models. A model is self-consistent and universal if it can approximate any other model and the inverse of any other model, including itself, with precision on the order of 0.01 pixels.

than other traditional models. So the polynomial model can also be used as a correction model by interchanging the role of distorted point coordinate and undistorted point coordinate in Eq. (1).

2.2 Plumb-line method

To correct the distortion from a single image, only the distorted points are available in general. In such case, some prior or implicit information is necessary to correct the distortion, for example, the extended epipolar geometry between corresponding distorted points [5, 17] or the prior shape of some image features [9]. The plumb-line method is based on the famous fact that a 3D line remains to be straight in 2D image if the camera is a pinhole camera (no lens distortion). Then the average distance from the edge points of a corrected line to their regression line is taken as the residual error of correction.

3 Test

In this section, we detail how to integrate the polynomial model into the plumb-line method and try different strategies to minimize the distortion. The synthetic test shows that the realistic distortion can be efficiently removed by using an appropriate minimization algorithm. In real test, the proposed method is compared to other methods and shows its higher correction precision.

3.1 Synthetic test

Given a set of corrected points $(x_{u_i}, y_{u_i})_{i=1, \dots, N}$ which are supposed to be on a line, we compute the linear regression line:

$$\alpha x_{u_i} + \beta y_{u_i} - \gamma = 0 \quad (2)$$

with $\tan 2\theta = -\frac{2(A_{xy} - A_x A_y)}{V_{xx} - V_{yy}}$, $\alpha = \sin \theta$, $\beta = \cos \theta$, $A_x = \frac{1}{N} \sum_{i=1}^N x_{u_i}$, $A_y = \frac{1}{N} \sum_{i=1}^N y_{u_i}$, $A_{xy} = \frac{1}{N} \sum_{i=1}^N x_{u_i} y_{u_i}$, $V_{xx} = \frac{1}{N} \sum_{i=1}^N (x_{u_i} - A_x)^2$, $V_{yy} = \frac{1}{N} \sum_{i=1}^N (y_{u_i} - A_y)^2$ and $\gamma = A_x \sin \theta + A_y \cos \theta$. The sum of squared distance from the points to this regression line is $\sum_{i=1}^N (\alpha x_{u_i} + \beta y_{u_i} - \gamma)^2$. By considering G groups of lines, the total sum of squared distance is:

$$S = \sum_{g=1}^G \sum_{l=1}^{L_g} \sum_{i=1}^{N_{gl}} S_{gli}^2 = \sum_{g=1}^G \sum_{l=1}^{L_g} \sum_{i=1}^{N_{gl}} (\alpha_g x_{u_{gli}} + \beta_g y_{u_{gli}} - \gamma_{gl})^2 \quad (3)$$

with L_g the number of lines in group g and N_{gl} the number of points of line l in group g and the total number of points $N = N_{11} + \dots + N_{1L_1} + \dots + N_{G1} + \dots + N_{GL_G}$. $(x_{d_{gli}}, y_{d_{gli}})$ the i -th distorted point on line l in group g and $(x_{u_{gli}}, y_{u_{gli}})$ the corresponding corrected point. The root mean squared distance is:

$$d = \sqrt{\frac{\sum_{g=1}^G \sum_{l=1}^{L_g} \sum_{i=1}^{N_{gl}} S_{gli}^2}{N}} \quad (4)$$

Polynomial model is chosen to correct the distorted lines. (x_c, y_c) can be fixed arbitrarily thanks to its invariance to the translation of distortion center. For the succinctness, the following discussion assumes a bicubic model with $p = q = 3$. Combine Eq. (1) and Eq. (3), the energy S becomes:

$$S = \sum_{g=1}^G \sum_{l=1}^{L_g} \sum_{i=1}^{N_{gl}} \left(\alpha_g (b_0 \bar{x}_{d_{gli}}^3 + \dots + b_9 + x_c) \right. \\ \left. + \beta_g (c_0 \bar{x}_{d_{gli}}^3 + \dots + c_9 + y_c) - \gamma_{gl} \right)^2 \quad (5)$$

It is a non-linear problem to minimize the energy S in parameters $b_0, b_1, \dots, c_0, c_1, \dots$. To have an idea what precision we can achieve, we first make this problem to be linear by assuming α_g, β_g are known. By derivating S to each parameter, we obtain a linear system:

$$\mathbf{A}\mathbf{x} = \mathbf{0} \quad (6)$$

with

$$\mathbf{x} = (\gamma_{11}, \dots, \gamma_{1L_1}, \dots, \gamma_{G1}, \dots, \gamma_{GL_G}, \\ b_0, \dots, b_9, c_0, \dots, c_9)^T.$$

\mathbf{A} is composed of 3 sub-matrix:

$$\mathbf{A} = \begin{bmatrix} \mathbf{A}_\gamma \\ \mathbf{A}_b \\ \mathbf{A}_c \end{bmatrix} \quad (7)$$

When there is only one group of lines, the rows of \mathbf{A}_b are proportional to the corresponding rows \mathbf{A}_c . So for test, we always use several groups of lines to avoid this situation. Yet the coefficient matrix is still singular since the last row of \mathbf{A}_b and the last row of \mathbf{A}_c are a linear combination of rows of \mathbf{A}_γ . This can be solved by fixing b_9 and c_9 to be 0. In this case, the coefficient matrix is non-singular and only one solution can be solved. But the solution is trivial because S is 0 by setting all the coefficients $b_1, \dots, b_9, c_1, \dots, c_9$ to 0 and $\gamma_{gl} = x_c \alpha_g + y_c \beta_g$. To avoid this trivial solution, we add a constraint that $b_7 = 1$ and $c_8 = 1$. This in fact introduces a scale to the solution and the fixed values of b_9 and c_9 introduce a translation to the solution. The minimized S can be changed by the introduced scale. But this change is consistent if $x_c, y_c, b_9, c_9, b_7, c_8$ are fixed. In the test, we use 8 groups of lines with orientations $10^\circ, 20^\circ, 30^\circ, 40^\circ, 50^\circ, 60^\circ, 70^\circ, 80^\circ$ to estimate the correction parameters by minimizing S . Once the parameters are estimated, another independent group of lines with orientation 55° is used for the verification. The ideal lines are distributed in image of size 1761×1174 . The sampling step of each line is 30 pixels and the number of samples on each lines are no less than 15. The distance between two adjacent lines is 30 pixels. The ideal lines

are distorted by radial distortion plus tangential distortion⁴. The correction result is recapitulated in Table 1. The precision on the order of 10^{-2} pixels can be achieved by increasing the order of polynomial model. An interesting phenomenon is that a pair of even order and odd order polynomial has almost the same precision. Fig. 1 shows ideal lines, distorted lines and corrected lines of the test group with orientation 55° . Remark that the corrected lines are close to the ideal lines but they do not completely superimpose due to the introduced translation and scale in the correction process. In fact, we can apply any rotation and translation on the corrected lines to obtain another groups of corrected lines, which gives the same residual error. However, applying a homography on the corrected lines can lead to different error depending on the scale introduced by the homography.

order $p = q$	d (in pixels) in Eq (4)	
	linear estimation	indep. measure
3	0.6935	0.6239
4	0.6096	0.5312
5	0.2439	0.2093
6	0.2419	0.2064
7	0.1050	0.0879
8	0.1031	0.0870
9	0.0521	0.0512
10	0.0515	0.0509
11	0.0477	0.0449
12	0.0474	0.0444

Table 1: Line correction with known orientation. The ideal lines are distorted by radial distortion plus tangential distortion (see footnote 4). The energy in Eq. (5) is minimized by using linear method. The root mean squared distance in Eq (4) is computed as measurement. Column 1 is the order of the polynomial model. Column 2 is the measurement for the lines with orientation from 10° to 80° . Column 3 is the measurement for the independent group of lines with orientation 55° .

In practice the orientation of lines is unknown. The minimization of the energy in Eq. (5) is a non-linear problem. Different strategies are tried to do this minimization. The first

⁴ The distortion is added according to the equation:

$$\begin{aligned}\bar{x}_d &= \bar{x}_u (k_0 + k_1 r_u + k_2 r_u^2 + \dots) \\ &+ [p_1 (r_u^2 + 2\bar{x}_u^2) + 2p_2 \bar{x}_u \bar{y}_u] (1 + p_3 r_u^2) + s_1 r_u^2 \\ \bar{y}_d &= \bar{y}_u (k_0 + k_1 r_u + k_2 r_u^2 + \dots) \\ &+ [p_2 (r_u^2 + 2\bar{y}_u^2) + 2p_1 \bar{x}_u \bar{y}_u] (1 + p_3 r_u^2) + s_2 r_u^2\end{aligned}$$

with k_0, k_1, \dots the radial distortion coefficients, p_1, p_2, p_3 the decentering distortion coefficients, s_1, s_2 thin prism distortion coefficients. In our synthetic test, $k_0 = 1.0$, $k_1 = 1.0e-4$, $k_2 = -2.0e-7$, $k_3 = 4.0e-10$, $k_4 = -6.0e-14$, $p_1 = 4.0e-6$, $p_2 = -2.0e-6$, $p_3 = 0$, $s_1 = 3.0e-6$, $s_2 = 1.0e-6$.

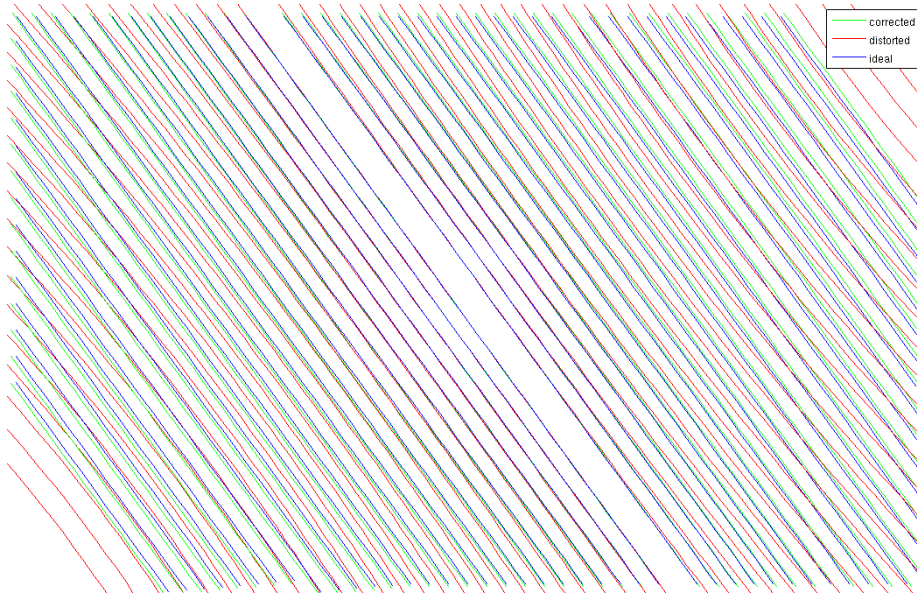


Figure 1: The corrected, distorted and ideal lines for the test group of lines with orientation 55° by using linear method. The green lines are corrected lines by using the estimated parameters; the red lines are distorted lines and the the blue lines are ideal lines.

strategy is simply Levenberg-Marquardt (LM) algorithm (see Table 2). But it is often stuck by a local minima. It works well only if the initialization is already close to the global minima. The second strategy is just to iterate the linear method to refine the orientation estimation of lines (see Table 3). The initial orientation is just the one of the regression line of the corresponding distorted points. The third strategy is to fix the orientation obtained by LM algorithm and do the iterative linear minimization to improve the result (see Table 2). The fourth strategy is the incremental LM algorithm followed by an iterative linear minimization. Incremental LM algorithm estimates the parameters of a high order polynomial model from low order model (see Table 4). For example, to estimate the parameters of a order-11 polynomial, we begin to estimate the parameters of a order-3 polynomial. Then the estimated order-3 parameters are used as the initialization for order-4 polynomial, and so on. This procedure is iterated until order-11. Finally a step of iterative linear minimization is added to improve the precision.

It is a difficult non-linear optimization problem to minimize the energy in Eq. (5) when the orientation of lines is unknown, in particular when the order of polynomial model is high. Comparing the results of different optimization strategies with the best precision we can obtain in Table 1, the incremental LM algorithm plus iterative linear method gives the closest performance.

order $p = q$	d (in pixels) in Eq (4)			
	estimation		indep. measure	
	LM	iter. linear	LM	iter. linear
3	0.7013	0.6489	0.5988	0.5596
4	0.6419	0.6109	0.5491	0.5087
5	0.2937	0.2852	0.2522	0.2507
6	0.2698	0.2624	0.2280	0.2222
7	0.2609	0.1509	0.1956	0.1452
8	0.3472	0.1611	0.2584	0.1574
9	0.2522	0.1503	0.2300	0.1561
10	0.9814	0.1863	0.5841	0.1763
11	0.5797	0.1593	0.4178	0.1454

Table 2: Line correction with unknown orientation by Levenberg-Marquardt (LM) algorithm and iterative linear method (strategy 1 and 3). The ideal lines are distorted by radial distortion plus tangential distortion (see footnote 4). The energy in Eq. (5) is minimized by LM algorithm plus a step of iterative linear minimization. The root mean squared distance in Eq (4) is computed as measurement. Column 1 is the order of the polynomial model. Column 2 is the measurement of LM algorithm (strategy 1) for the lines with orientation from 10° to 80° . Column 3 is the measurement of LM algorithm plus a linear minimization (strategy 3) for the lines with orientation from 10° to 80° . Column 4 and 5 corresponds to column 2 and 3 respectively, by using the the independent group of lines with orientation 55° which is not used for optimization.

order $p = q$	d (in pixels) in Eq. (4)	
	iter. linear	indep. measure
3	0.6315	0.5083
4	0.6136	0.4849
5	0.2601	0.2374
6	0.2594	0.2371
7	0.1469	0.1368
8	0.1455	0.1360
9	0.1105	0.1096
10	0.1106	0.1098
11	0.1156	0.1116

Table 3: Line correction with unknown orientation by iterative linear method (strategy 2). The ideal lines are distorted by radial distortion plus tangential distortion (see footnote 4). The energy in Eq. (5) is minimized by iterative linear minimization (strategy 2). The root mean squared distance in Eq. (4) is computed as measurement. Column 1 is the order of the polynomial model. Column 2 is the measurement of iterative linear minimization for the lines with orientation from 10° to 80° . Column 3 corresponds to column 2, by using the independent group of lines with orientation 55° which is not used for optimization.

3.2 Real test

The real experiments were made with a Canon EOS 30D reflex camera and an EFS 18 – 55mm lens. The minimal focal length (18mm) was chosen to produce a fairly large distortion. The RAW images were demosaicked by summing up the four pixels of each 2×2 Bayer cell, obtaining a half-size image. We built a pattern by tightly stretching strings on a wood frame, that guarantees straightness. This pattern looks like the harp, a musical instrument, where comes from the name “calibration harp”. Fig. ?? shows the distorted images of the harp with different orientations against the sky as background. The distortion is visible near the border of the image.

Before showing the correction result, we discuss how to extract the edge points of the distorted lines from the images in sub-pixel precision. Briefly, the lines are first detected by LSD algorithm which groups the pixels having coherent gradient direction into the line support region [20]. Then, in each validated line support region, Devernay’s algorithm [11] is used to extract the edge points in sub-pixel precision. Finally, a Gaussian convolution followed by a sub-sampling is performed on the extracted edge points to reduce the noise.

Line detection LSD is a linear-time line segment detector that gives accurate results, controlling number of false detections, and requires no parameter tuning [20]. The algorithm starts by computing the gradient direction at each pixel to produce a vector field. This vector field is segmented into con-

order $p = q$	d (in pixels) in Eq (4)			
	estimation		indep. measure	
	LM	iter. linear	LM	iter. linear
3	0.7042	0.6514	0.6018	0.5618
4	0.5995	0.5794	0.5128	0.4735
5	0.2571	0.2510	0.2219	0.2167
6	0.2463	0.2419	0.2093	0.2053
7	0.2126	0.1091	0.1740	0.0925
8	0.2067	0.1062	0.1661	0.0909
9	0.1953	0.0599	0.1569	0.0588
10	0.1823	0.0576	0.1425	0.0571
11	0.1805	0.0546	0.1419	0.0524

Table 4: Line correction with unknown orientation by incremental Levenberg-Marquardt (LM) algorithm and iterative linear method (strategy 4). The ideal lines are distorted by radial distortion plus tangential distortion (see footnote 4). The energy in Eq. (5) is minimized by incremental LM algorithm plus a step of iterative linear minimization. The root mean squared distance in Eq (4) is computed as measurement. Column 1 is the order of the polynomial model. Column 2 is the measurement of incremental LM algorithm for the lines with orientation from 10° to 80° . Column 3 is the measurement of incremental LM algorithm plus a linear minimization (strategy 4) for the lines with orientation from 10° to 80° . Column 4 and 5 corresponds to column 2 and 3 respectively, by using the the independent group of lines with orientation 55° which is not used for optimization.

nected regions of pixels that share the same orientation (up to a tolerance), called line support regions. Each line support region (a set of pixels) is a candidate for a line segment, which is then validated by a *contrario* approach and the Helmholtz principle proposed in [1, 2]. **More detail will be added by Rafael.**

Devernay’s detector LSD algorithm gives a validated line support region associated to a line segment, which groups a set of pixels sharing the same gradient orientation up to some toleration. Devernay’s detector [11] is then used to extract the edge points of the line segments with sub-pixel precision in each validated line support region. It is reported that Devernay’s detector can attain the precision about 0.05 pixels. The implementation of Devernay’s detector is very simple since it is derived from the well-known Non-Maxima Suppression method [7, 10]. It can be recapitulated in the following:

- Let a point (x, y) , where x and y are integers and $I(x, y)$ the intensity of pixel (x, y) .
- Calculate the gradient of image intensity and its magnitude in (x, y) .
- Estimate the magnitude of the gradient along the direction of the gradient in some neighborhood around (x, y) .
- If (x, y) is not a local maximum of the magnitude of the gradient along the direction of the gradient then it is not an edge point.
- If (x, y) is a local maximum then estimate the position of the edge point in the direction of the gradient as the maximum of an interpolation on the values of gradient norm at (x, y) and the neighboring points.

Remark that the sub-pixel refinement of Devernay’s detector is similar to the one of SIFT method [18] except that SIFT works on the Laplacian value and uses a two-dimension quadric interpolation, while Devernay’s detector works on the magnitude of gradient and uses a one-dimension quadric interpolation in the gradient direction.

Convolution and sub-sampling of edge points For the photos of strings, almost every pixel along each side of one string is detected as edge point in sub-pixel precision. With more than 10 strings longer than 1000 pixels in 20 photos, there are about 400000 edge points in total. This large number of edge points can make the minimization of the energy in Eq. (5) very long. A convolution followed by a sub-sampling can be used to reduce the number of edge points. This process is similar to the two-dimension case where the Gaussian blur about $0.8 \times \sqrt{t^2 - 1}$ is needed before a t -subsampling to avoid the aliasing [15]. The similar rule can be applied here. But instead of a two-dimension signal, we have two one-dimension signals (x -coordinate and y -coordinate of edge points) along the length of the line. The Gaussian convolution is performed on two one-dimension signals separately. Since the edge points are not regularly sampled along the line, a preliminary step

of re-sampling is needed. This re-sampling is also along the length of the line by taking an uniform sampling step, which is set to be m times smaller than the average distance between two adjacent edge points. A linear interpolation is used here to do the re-sampling fast (see Fig. 2). Assume the distance between two adjacent edge points (x_1, y_1) and (x_2, y_2) is l and the re-sampling step is d . Then the re-sampled point (x', y') can be expressed as:

$$\begin{aligned} x' &= \frac{d}{l}(x_2 - x_1) + x_1 \\ y' &= \frac{d}{l}(y_2 - y_1) + y_1. \end{aligned}$$

Once the line is re-sampled, the Gaussian blur $0.8 \times \sqrt{t^2 - 1}$ can be applied then followed by a sub-sampling of factor mt on x and y coordinate separately (the re-sampling step is m times smaller than the average distance between two adjacent edge points).

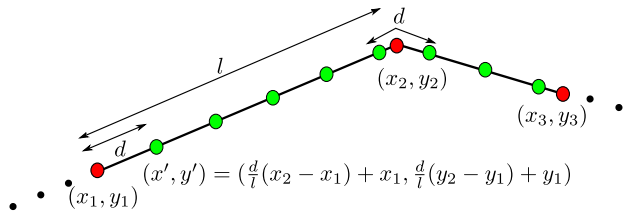


Figure 2: Line re-sampling. The red points (x_1, y_1) , (x_2, y_2) , \dots are the edge points extracted by Devernay's detector. They are irregularly sampled along the line. The re-sampling (in green) is along the length of the line with the uniform step d . The linear interpolation is used to compute the re-sampled point fast.

Once the edge points associated to the distorted line segments are extracted in sub-pixel precision, they can be directly integrated into the energy term in Eq. (5). According to the performance of different strategies in synthetic test, we only try the incremental LM followed by iterative linear minimization. All the distorted lines in Fig. 3 are used in the minimization with a polynomial model of order 11. An independent distorted image is used for verification. The correction result is recapitulated in Fig. 4.

Different methods, like the non-parametric method in Chapter ?? [14], Lavest *et al.* calibration method [16] and an iterative linear plumb-line method [3], are also tried (see the correction precision in Table 5). The non-parametric method in [14] estimates the distortion as the diffeomorphism (up to a homography) mapping the original digital pattern to a photograph of it by triangulating and interpolating dense correspondences (see result in Fig. 5). The Lavest *et al.* calibration method [16] is similar to global camera calibration methods

except that it assume that pattern is not flat and estimates also the 3D position of the feature points on the pattern (see result in Fig. 6). Alvarez’s iterative linear plumb-line method [3] uses a pure radial distortion model and minimizes the variance of distance from the corrected points to their regression line by iterative linear method (see result in Fig. 8). Like the real experiments in Chapter ??, we can also use the polynomial model to approximate the mapping between the digital pattern and its photo, instead of triangulation and affine interpolation used in Chapter ?? [14] (see result in Fig. 7). The correction precision, computed as the RMS distance from the edge points on the corrected line to their regression line, is recapitulated in Table 5 for different methods.

It seems that two plumb-line based methods (Alvarez *et al.* method and the proposed one) give the precision better than the other methods. This is not surprising because on the one hand the two methods explicitly minimize the straightness error of corrected lines; on the other hand, the two methods do not suffer from the error compensation in global calibration methods or the non-flatness of pattern in non-parametric method. The disadvantage of Alvarez *et al.* method is that it uses a simple radial distortion model with distortion center fixed at the center of image to get an iterative linear solution. But this model is not enough general to explain real distortion. This explains why Alvarez *et al.* method corrects some lines less precisely than the other ones.

For Lavest *et al.* method, the minimized re-projection error is about 0.02 pixels, while the corrected lines do not have that precision (see Fig. 6). This can only be explained by the error compensation between camera internal and external parameters. For the non-parametric method, a global tendency in the straightness error of the corrected lines can be observed (Fig. 5). This was in fact due to the unavoidable drawback of this method: there is never a guarantee that the pattern is completely flat. The non-flatness of the pattern introduces a bias in the estimated distortion field, which causes the observable global distortion in the plotted curves in Fig. 5. Remark that the very similar global tendency can be observed when the distortion is approximated by a 11-order polynomial instead of triangulation and affine interpolation (see Fig. 7).

To eliminate this error source, the solution is either to construct a very flat pattern, or to recover the 3D shape of a non-flat pattern. But neither is very feasible in practice. In contrast, to appropriately use a plumb-line method, we need a pattern containing very straight lines, and this is far easier in practice. As shown in Fig. 4, the distortion correction is so accurate that no global tendency is visible in corrected curves. The root mean square (RMS) distance of each line is also significantly smaller than for the non-parametric method (Table 5). It is particularly striking in Fig. 4 that the superimposed curves of the left and right side of each string are fairly uncorrelated, meaning that no deterministic distortion is left. The erratic oscillation of very small amplitude can be attributed to any cause, from the lack of the uniformity of the

harp background causing a shift in the edge detection, to the inhomogeneous blur in the image itself or the quality of strings. But it cannot be due to a residual mismatch of the polynomial model itself, because otherwise the curves on both sides of each string would be parallel. This confirms *a posteriori* the reliability of the polynomial model.

The estimated distortion field of the above methods are also different. For the non-parametric method, the distortion field consists of the vectors pointing from a certain point in the undistorted image to its correspondence in the distorted image. So an undistorted image can be directly obtained given a distorted image. Remark that the non-parametric method estimates the distortion field up to an unknown homography. So the distortion field is largely different from radial symmetric. For all the other methods, the distortion parameters are estimated from the distorted image to the undistorted image. But this correction model does not necessarily send all the points in distorted image to cover all the integer-position points of undistorted image domain. So the resulted undistorted image can contain holes. This problem can be solved by either reversing the model or computing the corresponding distorted point in the distorted image for the integer-position point in the corrected image by non-linear minimization, followed by an image interpolation. The radial model with known distortion center (used in Alvarez *et al.* method) is invertible. But this inversion is point by point and does not give an explicit formula of the inverse model. In contrast, the inverse polynomial model (distortion model) can be easily computed explicitly. Given a polynomial model (correction model), an arbitrary set of distorted points and corrected points can be generated. From these points, the coefficients of the inverse model in Eq. (1) can be estimated by linear method:

$$\begin{bmatrix} \vdots & \vdots & \vdots & \ddots & \vdots & \vdots & \vdots & \vdots & \ddots & \vdots \\ \bar{x}_{u_i}^p & \bar{x}_{u_i}^{p-1}\bar{y}_{u_i} & \bar{x}_{u_i}^{p-2}\bar{y}_{u_i}^2 & \cdots & 1 & 0 & 0 & 0 & \cdots & 0 \\ 0 & 0 & 0 & \cdots & 0 & \bar{x}_{u_i}^q & \bar{x}_{u_i}^{q-1}\bar{y}_{u_i} & \bar{x}_{u_i}^{q-2}\bar{y}_{u_i}^2 & \cdots & 1 \\ \bar{x}_{u_{i+1}}^p & \bar{x}_{u_{i+1}}^{p-1}\bar{y}_{u_{i+1}} & \bar{x}_{u_{i+1}}^{p-2}\bar{y}_{u_{i+1}}^2 & \cdots & 1 & 0 & 0 & 0 & \cdots & 0 \\ 0 & 0 & 0 & \cdots & 0 & \bar{x}_{u_{i+1}}^q & \bar{x}_{u_{i+1}}^{q-1}\bar{y}_{u_{i+1}} & \bar{x}_{u_{i+1}}^{q-2}\bar{y}_{u_{i+1}}^2 & \cdots & 1 \\ \vdots & \vdots & \vdots & \ddots & \vdots & \vdots & \vdots & \vdots & \ddots & \vdots \end{bmatrix} \begin{pmatrix} b_0 \\ \vdots \\ b_{\frac{(p+1)(p+2)}{2}-1} \\ c_0 \\ \vdots \\ c_{\frac{(q+1)(q+2)}{2}-1} \end{pmatrix} = \begin{pmatrix} \vdots \\ \bar{x}_{d_i} \\ \bar{y}_{d_i} \\ \bar{x}_{d_{i+1}} \\ \bar{y}_{d_{i+1}} \\ \vdots \end{pmatrix}$$

One pair of distorted point and undistorted point gives two equations. So at least $\frac{(p+1)(p+2)}{4} + \frac{(q+1)(q+2)}{4}$ pairs of correspondences are required to estimate the parameters.

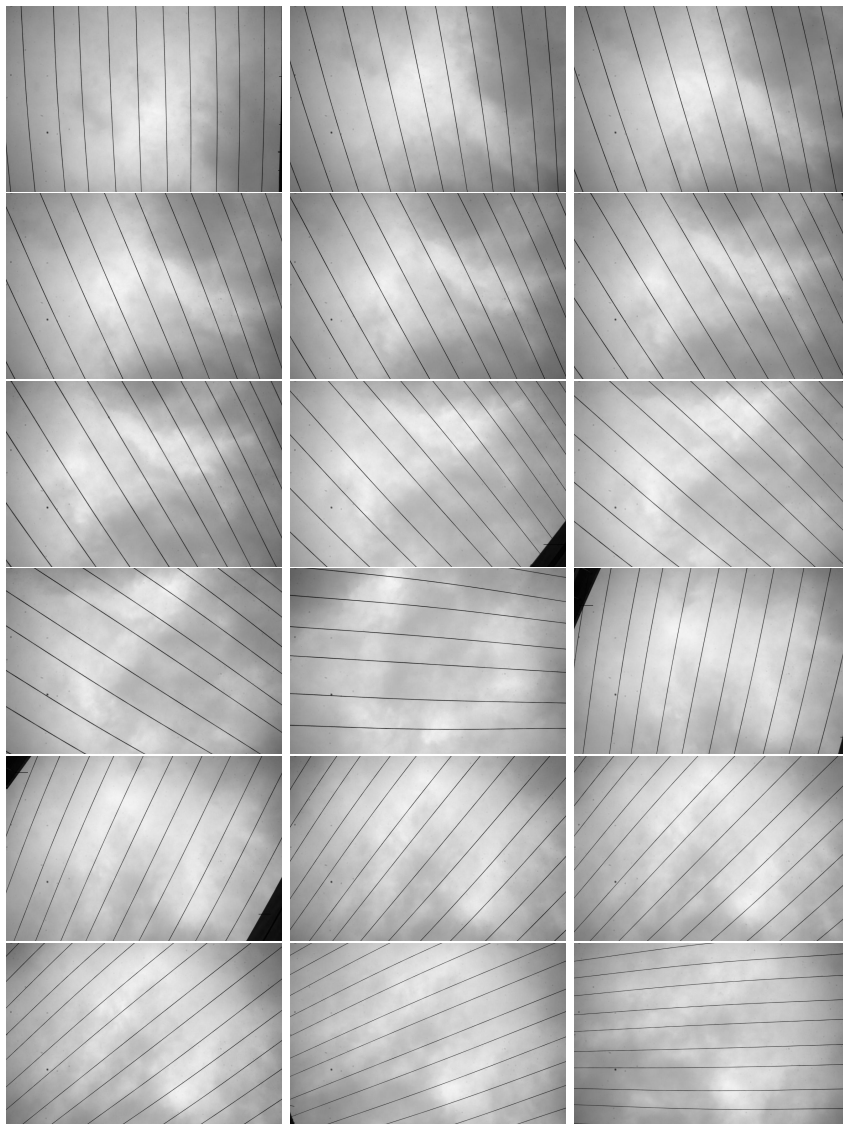


Figure 3: Distorted sewing strings taken by the camera by hand with different orientations.

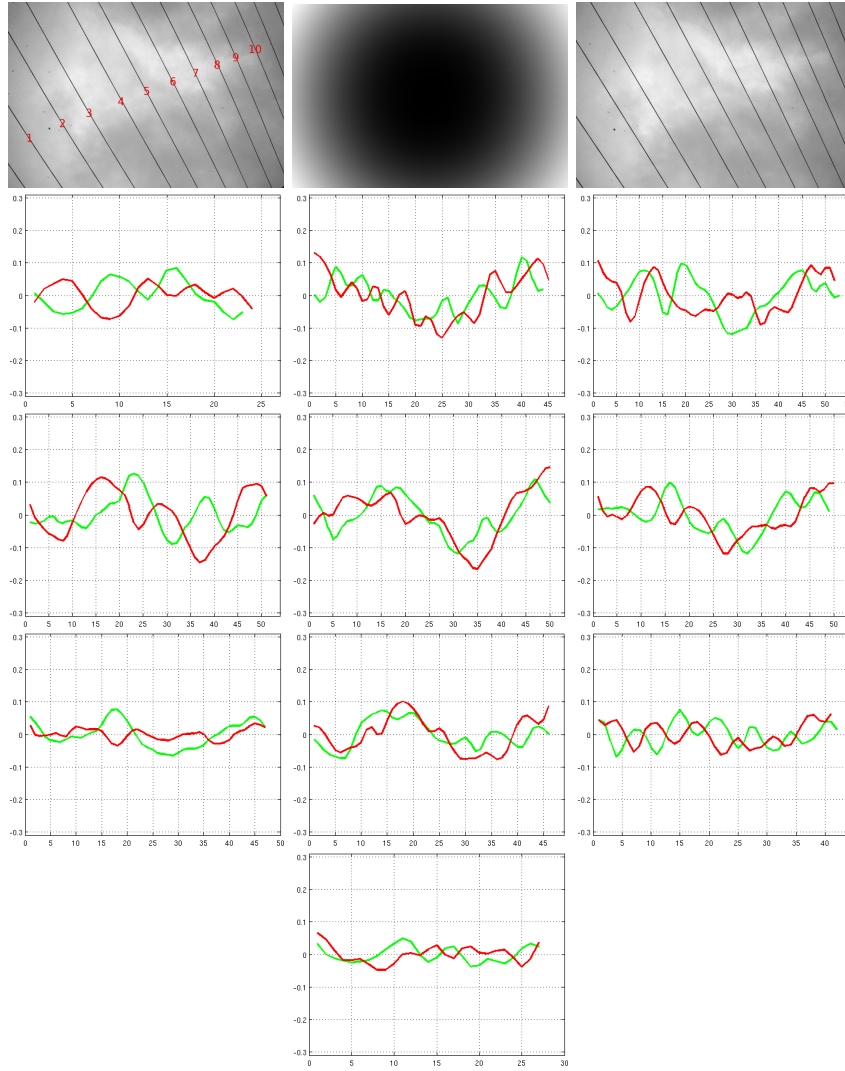


Figure 4: Correction performance of the proposed plumb-line based method with calibration harp. The first row, from left to right: the independent distorted image, the distortion field and the corrected image. From the second row to the last row, from left to right: the distance in pixels from the edge points to their regression line on line 1 to 10 in the distorted image on top-left, after correction. Note each figure contains two curves because there are two sides for one line.

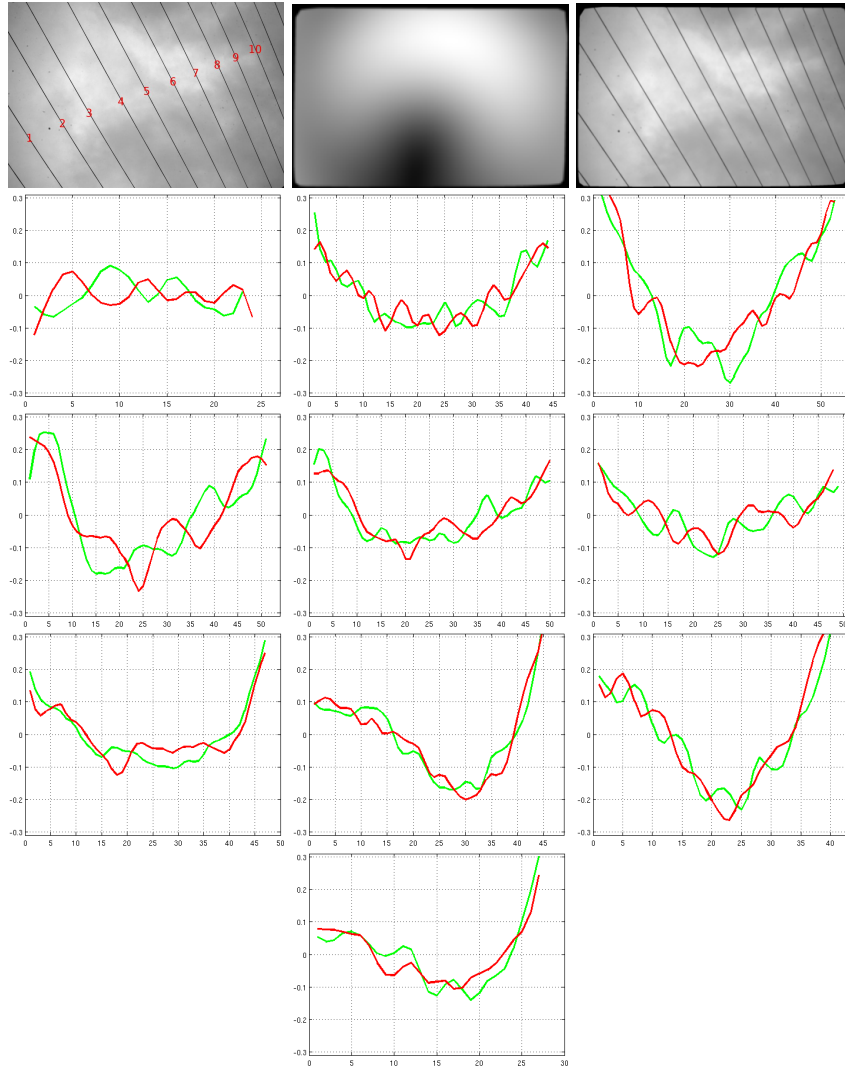


Figure 5: Correction performance of the non-parametric pattern-based method [14]. The first row, from left to right: the independent distorted image, the distortion field and the corrected image. From the second row to the last row, from left to right: the distance in pixels from the edge points to their regression line on line 1 to 10 in the distorted image on top-left, after correction. Note each figure contains two curves because there are two sides for one line.

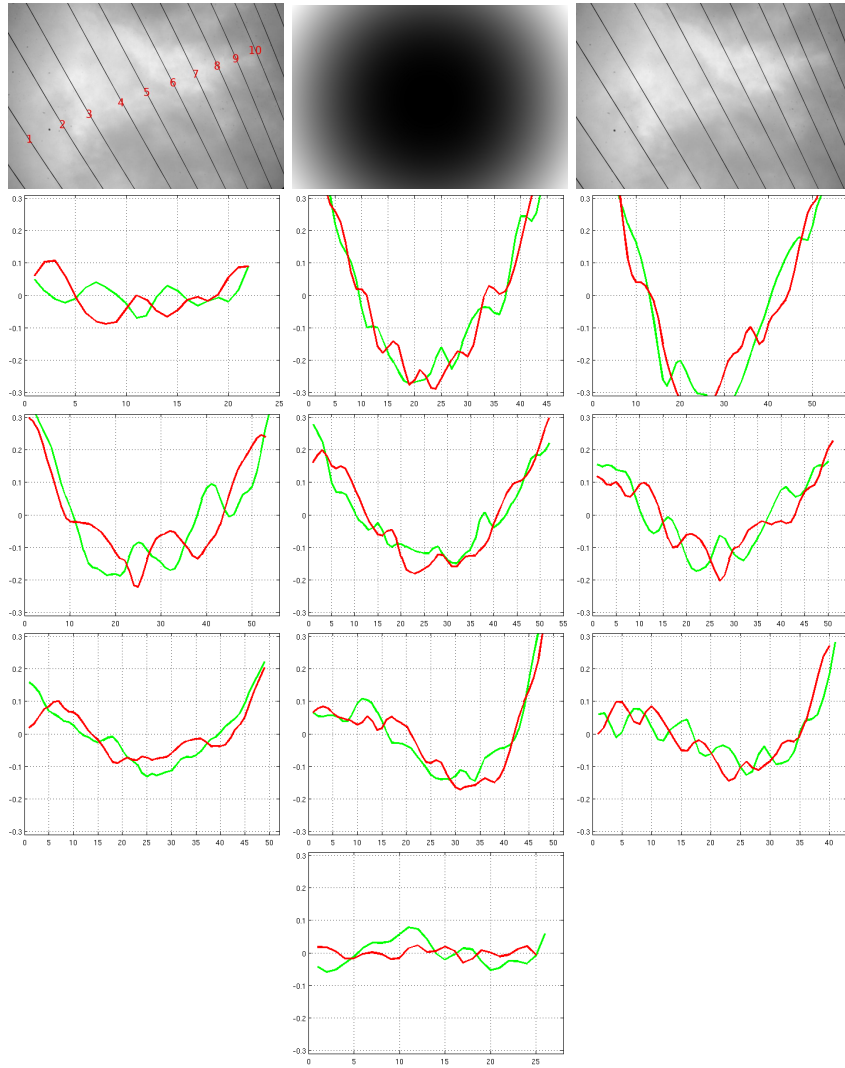


Figure 6: Correction performance of Lavest *et al.* method [16]. The first row, from left to right: the independent distorted image, the distortion field and the corrected image. From the second row to the last row, from left to right: the distance in pixels from the edge points to their regression line on line 1 to 10 in the distorted image on top-left, after correction. Note each figure contains two curves because there are two sides for one line.

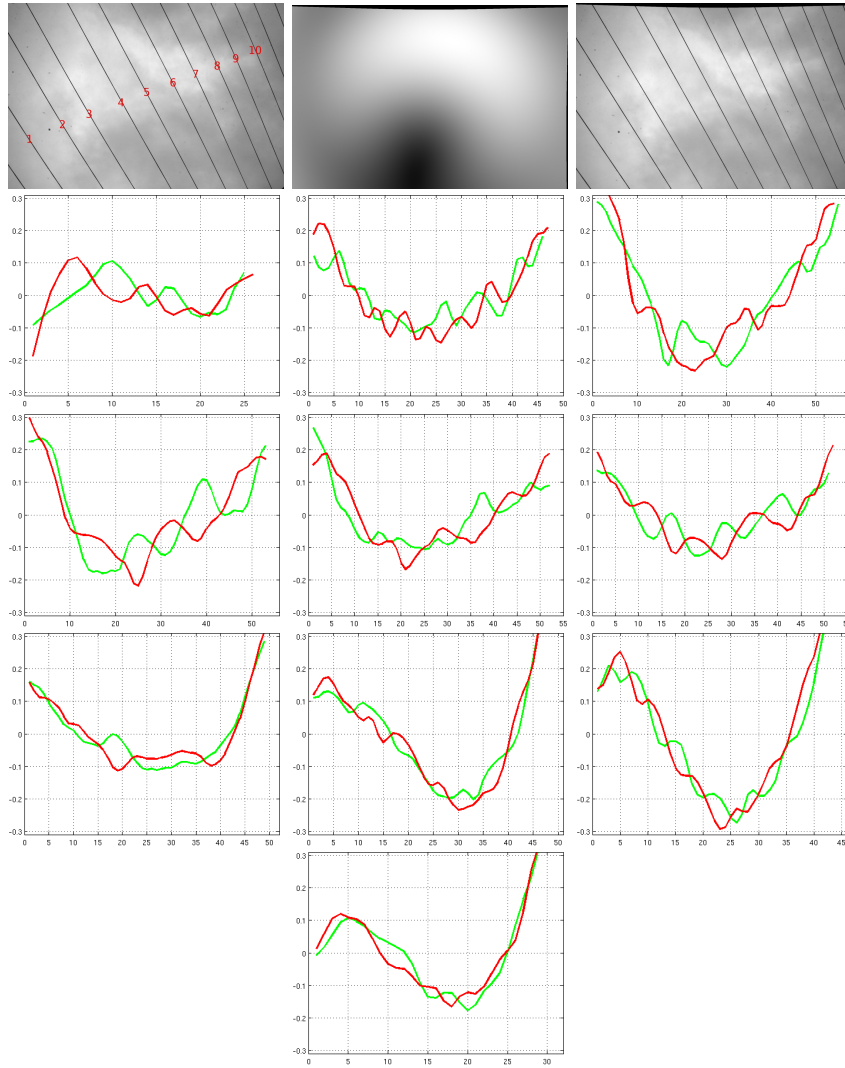


Figure 7: Correction performance of textured pattern with polynomial. The first row, from left to right: the independent distorted image, the distortion field and the corrected image. From the second row to the last row, from left to right: the distance in pixels from the edge points to their regression line on line 1 to 10 in the distorted image on top-left, after correction. Note each figure contains two curves because there are two sides for one line.

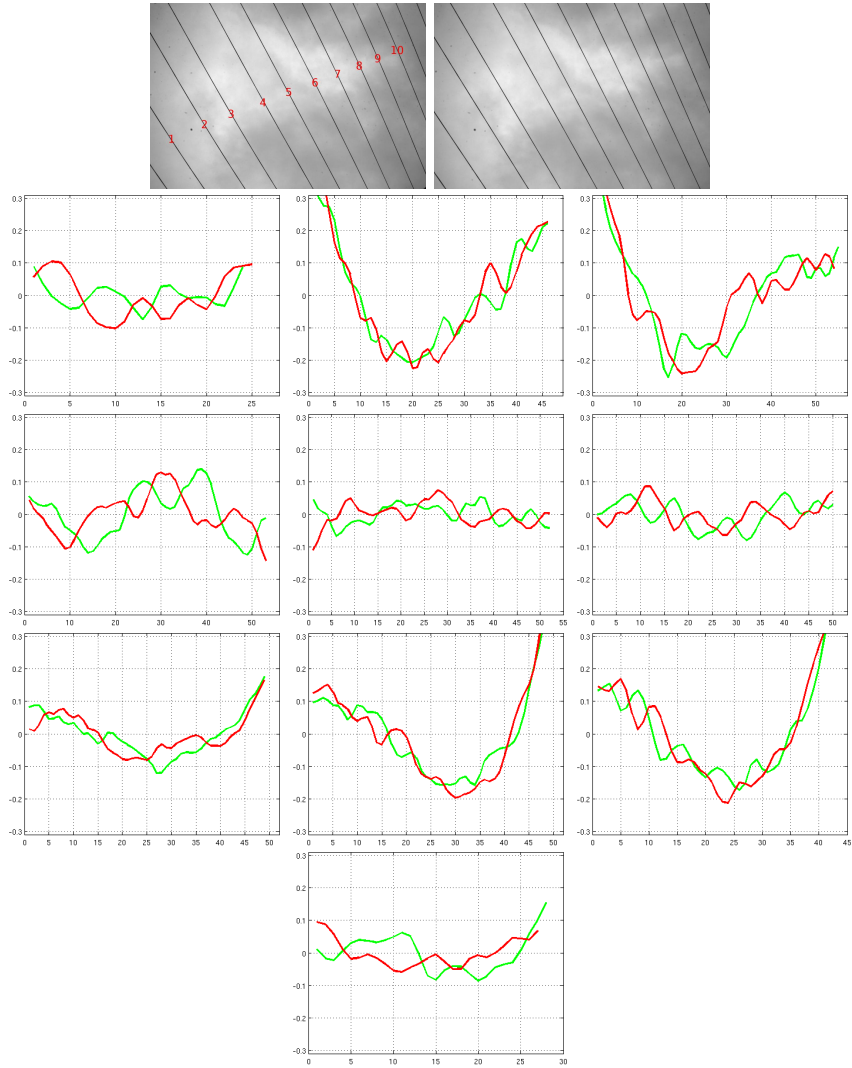


Figure 8: Correction performance of Alvarez *et al.*. The first row, from left to right: the independent distorted image and the corrected image. From the second row to the last row, from left to right: the distance in pixels from the edge points to their regression line on line 1 to 10 in the distorted image on top-left, after correction. Note each figure contains two curves because there are two sides for one line.

line No.	RMSE (in pixels)				
	polynomial model	non-parametric [14]	Lavest method	polynomial textured pattern	Alvarez method
1	0.046/0.036	0.048/0.042	0.035/0.062	0.055/0.065	0.038/0.069
2	0.050/0.068	0.088/0.082	0.217/0.218	0.081/0.112	0.157/0.171
3	0.057/0.054	0.166/0.168	0.267/0.270	0.152/0.174	0.147/0.152
4	0.051/0.073	0.135/0.126	0.156/0.139	0.129/0.128	0.076/0.060
5	0.061/0.076	0.082/0.080	0.118/0.137	0.092/0.103	0.029/0.035
6	0.052/0.056	0.069/0.062	0.108/0.099	0.075/0.088	0.041/0.037
7	0.039/0.017	0.095/0.080	0.090/0.072	0.100/0.102	0.067/0.058
8	0.042/0.054	0.133/0.143	0.117/0.127	0.163/0.180	0.129/0.152
9	0.035/0.036	0.154/0.162	0.080/0.095	0.197/0.204	0.131/0.146
10	0.099/0.082	0.040/0.014	0.122/0.120	0.058/0.043	0.058/0.043

Table 5: RMS distance from edge points of corrected lines to their corresponding regression line. The proposed method is compared to non-parametric pattern-based method [14], Lavest *et al.* method, textured pattern polynomial fitting method and Alvarez method. Note that each cell in table contains two values because there are two sides for one line. The lines are numerated in the top-left image in Fig. 4.

4 How to improve?

As explained before, the main motivation to build a “calibration harp” for distortion correction is to detour the difficult in obtaining a very flat pattern with flatness error on the order of 10 micron. Even though it is easier to build a “calibration harp” with tightly stretched strings, the quality of strings plays an important role. In the previous experiments, the sewing strings are used to build the “calibration harp”. But the sewing string is not very smooth and the thickness varies along the string due to its twisted structure (see Fig. 10a). All these defects can pose problem to the high-precision extraction of the edge points from the photos of the strings and thus motivate us to find the string of better quality. Besides the sewing string, the tennis string (Fig. 10b) and the fishing string (Fig. 10c) are also tried in the experiments. Among the three types of string, the tennis string and the fishing string are more smooth than the sewing string and have the thickness more uniform. But it is difficult to stretch the tennis string to make it very straight due to its rigidity. To improve the quality of strings, finally we choose the flexible fishing strings and stretch them tightly on a wood framework (see Fig. 9).

To ensure the extraction precision of the edge points from the string images, we prefer an uniform background which is in contrast with the string color. The first idea is naturally to use an uniform wall as the background. But the shadow of the strings can make the edge points detector fail. A background which does not have the shadow of the strings should be far away from the harp. So the sky is the only distant and uniform background we can find. But in the experiments, we found that it is difficult to take the photos of the harp against the sky.

When the angle of view of the camera is large, it is difficult to avoid the environment around (like buildings, trees, etc) in the photos. In addition, the sky is rarely uniform (the sky can be seen as some clouds randomly distributed on the blue background, for example see the images in Fig. 3 or Fig. 11a). The final solution we found is to install a semi-transparent paper on the back of the harp. The semi-transparent paper blocks the camera to see the other objects than the strings and let the light come from the back to avoid the shadow (see Fig. 9b for the harp with the semi-transparent paper). This setup allows us to take photos more freely by putting the harp anywhere there is enough light coming from the back.

The Canon EOS 30D reflex camera is installed on the tripod with 10 seconds timer to avoid the hand vibration. Photos of different orientations are taken by rotating the camera on the tripod. The camera is always parallel to the harp and has the same distance to the harp (see Fig. 13 for photos of different orientations). Compared to the photos of sewing strings taken by hand against the sky (Fig. 11a), the photos of fishing strings with a semi-transparent paper (Fig. 11b) have a more uniform background. In addition, the images taken by hand (Fig. 11a) suffers from inhomogeneous blur or variation of strings thickness caused by the inconstant distance from camera to the harp or the hand motion, while the images taken by tripod have better quality.

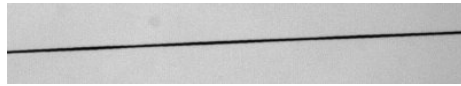


(a) The harp with an uniform opaque object as background

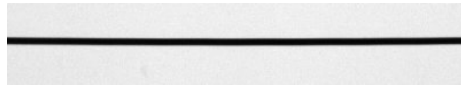
(b) The harp with a semi-transparent paper as background

Figure 9: The harp with an opaque object or a semi-transparent paper as background. (a) The harp with an uniform opaque object as background. (b) The harp with a semi-transparent paper as background.

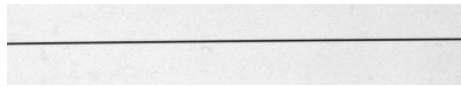
The improvement of the string quality and the photo quality leads to a better correction performance. As we have seen before, even though the plumb-line method with a polynomial model can correct the distortion up to about 0.05 pixels (Fig. 4) and no big global tendency can be observed, the maximal amplitude of oscillation can still be as big as 0.05 pixels. For the second line in Fig. 4, the small global tendency is observed. But the amplitude of this small global tendency is on the same order of the amplitude of oscillation. So the minimization algorithm



(a) The sewing line



(b) The tennis line

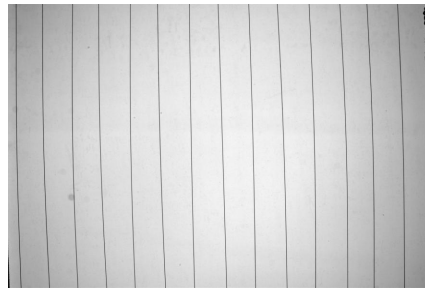


(c) The fishing line

Figure 10: The quality of lines. (a) sewing line. (b) tennis line. (c) fishing line.



(a) The photo of harp is taken against the sky by hand



(b) The photo of harp is taken against a semi-transparent paper by a tripod

Figure 11: The quality of photos depends on the harp, its background and also the stability of camera for taking photos.

cannot tell apart the two types of error. In such situation, it is possible that the minimization algorithm pays more attention to minimize the oscillation than the global tendency. So it is ideal to have the oscillation as small as possible such that the minimization algorithm can concentrate on the the global tendency minimization. The oscillation is not the distortion property of the camera lens. Instead it is related to the quality of lines. More concretely, the oscillation inherits the high frequency of the distorted lines, while the distortion stands for the low frequency of the distorted lines. In Fig. 12, the high frequency of distorted sewing string, distorted tennis string and distorted fishing string is compared to the straightness error of their corresponding corrected string. The almost superimposed oscillation proves the inheritance from the high frequency of distorted strings. Among the three types of strings, the fishing string shows the smallest oscillation. The bigger oscillation of the sewing string is due to the variation of the thickness related to the twisted structure, while the tennis string suffers from its rigidity which makes it difficult to be stretched straight (even though visually it is stretched straight in Fig. 10b).

With the fishing strings harp, the same experiments as the sewing strings harp were performed. Here we do not do a comprehensive comparison with the the methods and only concentrate on the improvement of precision by using a harp of fishing strings. In the Fig. 14, the straightness error is shown in the same form as before. Compared to Fig. 4, it is evident that we have a more precise correction and the residual oscillation is reduced.

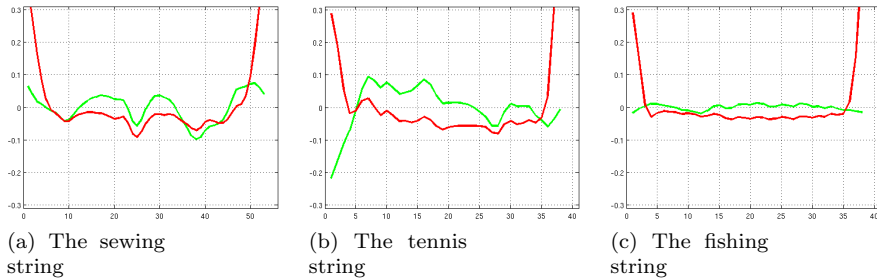


Figure 12: The small oscillation of the corrected lines is related to the quality of lines. The green curve shows the RMS distance (in pixels) from the edge points of a corrected line to its regression line. The red curve shows the high frequency of the corresponding distorted line. The corrected line will inherit the oscillation from the corresponding distorted line. (a) the sewing string. (b) the tennis string. (c) the fishing line. The x -axis is the index of edge points. The range of y -axis is from -0.3 pixels to 0.3 pixels.

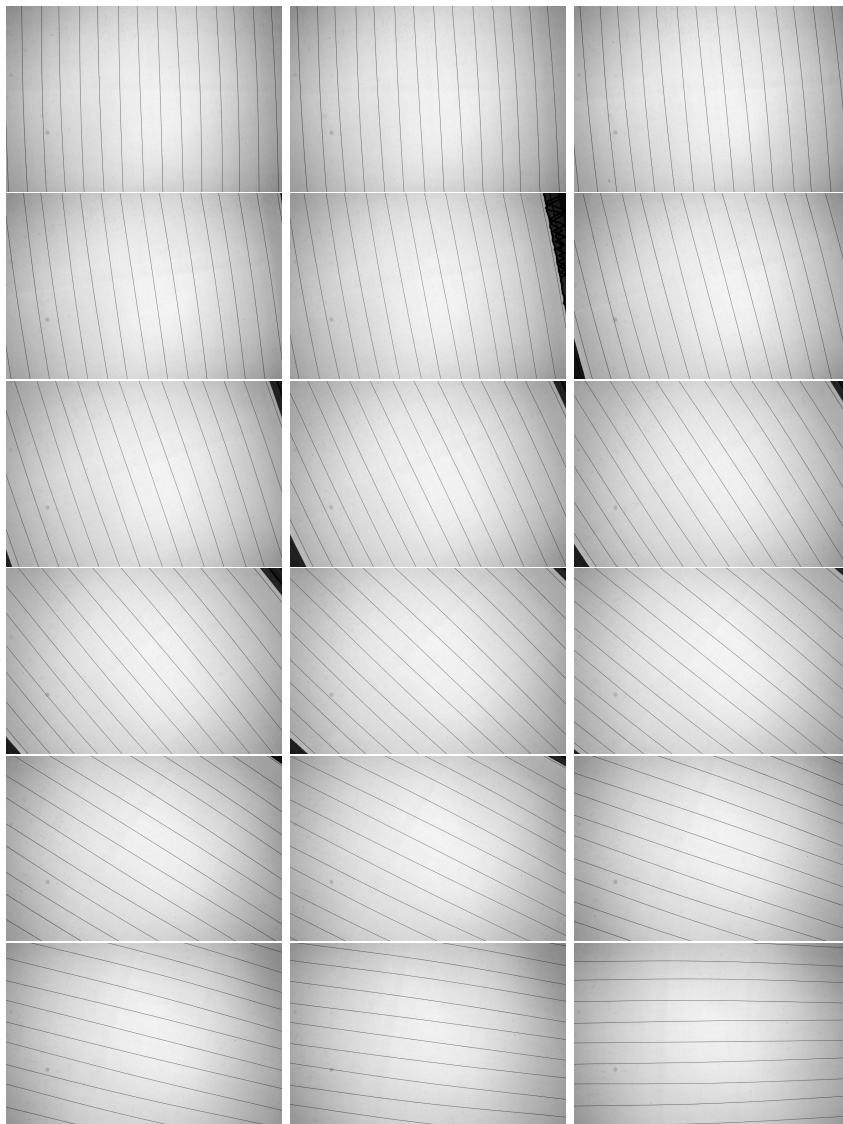


Figure 13: Distorted fishing strings taken by the camera fixed on a tripod with different orientations.

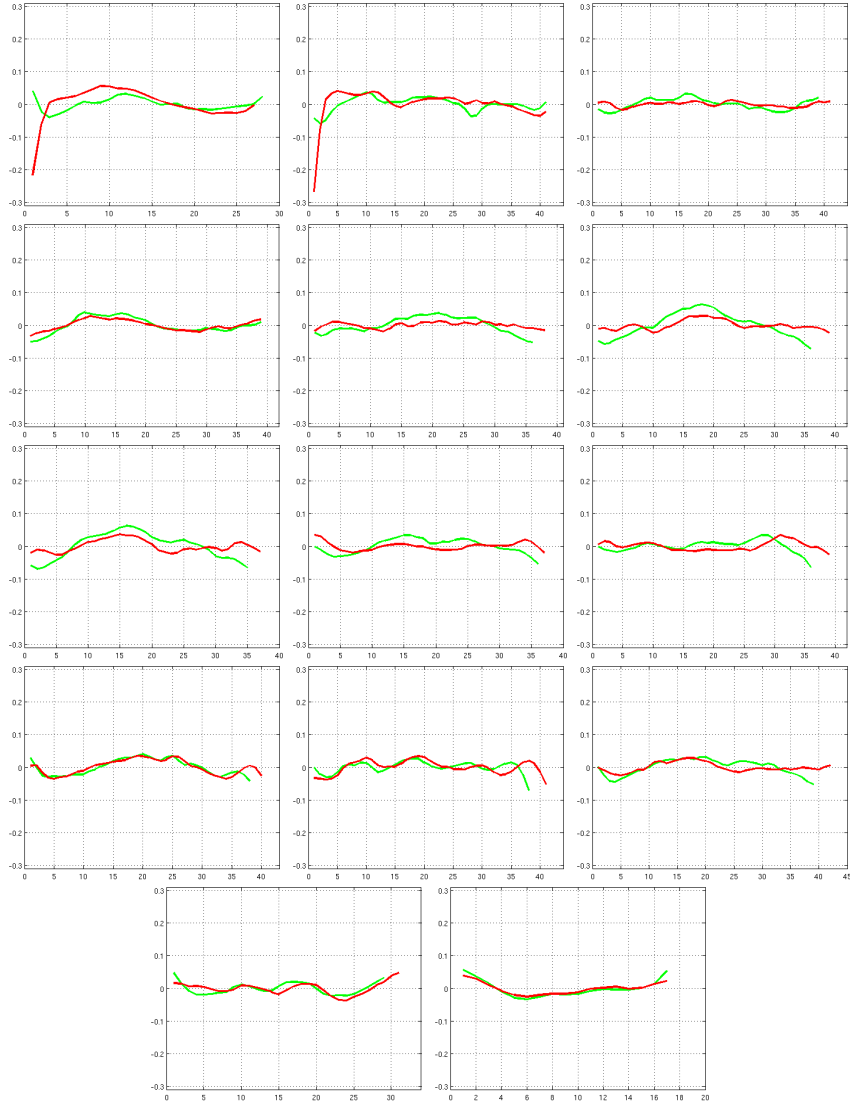


Figure 14: Correction performance of the proposed plumb-line based method with a harp made up of fishing strings. The x -axis is the index of edge points. The range of y -axis is from -0.3 pixels to 0.3 pixels.

5 The correction performance of global camera calibration is unstable

We have shown a correction example of global camera calibration method (Lavest *et al.* method). It does not correct the distortion as well as the plumb-line based method (see the comparison in Table 5 or Fig. 4 and Fig. 6). A more important drawback of global camera calibration is that it does not give a stable correction due to the error compensation among many parameters. When different distortion models are used in the global calibration, different corrections will be obtained. This is an annoying problem because *a priori* we do not know which distortion model and which parameters are more appropriate for a certain camera. The results in Fig. 6 are obtained by using the Brown’s classic distortion model [6] with 2 radial parameters and 2 tangential parameters in Lavest *et al.* method. Table 6 compares the correction precision by using different number of distortion parameters. It is clear that the correction precision varies and we have the best precision by using 5 radial parameters.

line No.	RMSE (in pixels)			
	2 radial params	5 radial params	2 radial + 2 tangent	5 radial + 2 tangent
1	0.038/0.068	0.032/0.061	0.035/0.062	0.031/0.057
2	0.172/0.173	0.139/0.140	0.217/0.218	0.172/0.175
3	0.190/0.191	0.154/0.160	0.267/0.270	0.219/0.220
4	0.101/0.087	0.099/0.089	0.156/0.139	0.131/0.115
5	0.068/0.085	0.062/0.077	0.118/0.137	0.086/0.106
6	0.055/0.042	0.044/0.035	0.108/0.099	0.076/0.066
7	0.023/0.054	0.029/0.028	0.090/0.072	0.085/0.057
8	0.085/0.072	0.064/0.048	0.117/0.127	0.085/0.103
9	0.073/0.062	0.060/0.036	0.080/0.095	0.073/0.083
10	0.057/0.039	0.047/0.027	0.122/0.120	0.030/0.014

Table 6: The RMSE of corrected lines under estimated parameters by Lavest *et al.* method with different number of distortion parameters.

6 Conclusion

By combining the advantages of a model-free polynomial approximation and of a real plumb line pattern, the proposed lens distortion correction is significantly more accurate than parametric methods on flat patterns. The “calibration harp” construction only requires the acquisition of a string with decent quality. It is far simpler than realizing a flat plate with highly accurate patterns engraved on it. (The calibration of such patterns is not easier than lens calibration itself!) The high number of degrees of freedom in the unstructured model explains why we can call the method model-free. The only assumption on the lens distortion is its smoothness, implying

that a polynomial with high enough order approximates it. In our experiments, the approximation error stabilizes for polynomials of degree 7 to 11. It might be objected that the high number of parameters in the polynomial interpolation (156 for an 11-order polynomial) could cause some bias in the result. Yet, the number of control points is far higher: There were about 10 strings for each orientation, some 30 control points on each string side, and some 18 orientations. Thus the number of control points is about 10000 and therefore 60 times more than the number of polynomial coefficients. A visual examination of the two sides of the strings confirms that no artificial simultaneous bias has been introduced by the polynomial distortion correction. This observation seems to indicate that most of the 0.05 pixels remaining oscillation is due either to image processing factors, or to background inhomogeneity, to aliasing in the edge detector, or to string diameter variations. By building a harp of better quality with fishing strings, we do gain a factor about 2 even 3. We also show that the global camera calibration is not reliable to correct the distortion.

References

- [1] Jean-Michel Morel Agnès Desolneux, Lionel Moisan. Meaningful alignments. *International Journal of Computer Vision*, 40(1):7–23, 2000.
- [2] Jean-Michel Morel Agnès Desolneux, Lionel Moisan. *From Gestalt Theory to Image Analysis, a Probabilistic Approach*. Springer, 2008.
- [3] Luis Alvarez and J. Rafael Sendra. An algebraic approach to lens distortion by line rectification. *Journal of Mathematical Imaging and Vision*, 35:36–50, 2009.
- [4] T. Pajdla B. Micusik. Estimation of omnidirectional camera model from epipolar geometry. *CVPR*, 1:485, 2003.
- [5] K. Barreto, J.P. Daniilidis. Fundamental matrix for cameras with radial distortion. *ICCV*, 1:625–632, 2005.
- [6] Duane C. Brown. Close-range camera calibration. *Photogrammetric Engineering*, 37:855–866, Brown.
- [7] J. F. Canny. Finding edges and lines in images. *Technical Report AI-TR-720, Massachusetts Institute of Technology, Artificial Intelligence Laboratory*, 1983.
- [8] D. Claus and A.W. Fitzgibbon. A rational function lens distortion model for general cameras. *CVPR*, 1:213–219, 2005.
- [9] Margaret M. Fleck Daniel Stevenson. Nonparametric correction of distortion. Technical report, omp. Sci., U. of Iowa, 1995.
- [10] R. Deriche. Using canny's criteria to derive a recursively implemented optimal edge detector. *The International Journal of Computer Vision*, 1(2):167187, 1987.
- [11] F. Devernay. A non-maxima suppression method for edge detection with sub-pixel accuracy. Technical Report 2724, INRIA rapport de recherche, 1995.

- [12] F. Devernay and O. Faugeras. Straight lines have to be straight. *Mach. Vision Appl.*, 13:14–24, 2001.
- [13] A. Fitzgibbon. Simultaneous linear estimation of multiple view geometry and lens distortion. *ICPR*, 1:125–132, 2001.
- [14] R. Grompone von Gioi, P. Monasse, J.-M. Morel, and Z. Tang. Towards high-precision lens distortion correction. *ICIP*, pages 4237–4240, 2010.
- [15] Guoshen Yu Jean-Michel Morel. On the consistency of the sift method. Technical report, CMLA, ENS-Cachan, 2008.
- [16] Dhome M. Lavest J., Viala M. Do we really need accurate calibration pattern to achieve a reliable camera calibration. *ECCV*, 1:158–174, 1998.
- [17] Hongdong Li and Richard Hartley. A non-iterative method for correcting lens distortion from nine point correspondences. *OmniVis*, 2005.
- [18] David G Lowe. Distinctive image features from scale-invariant keypoints. *IJCV*, 60(2):91110, 2004.
- [19] J.-M. Morel R. Grompone von Gioi and Z. Tang. Self-consistency and universality of camera lens distortion models. *CMLA Preprint, ENS-Cachan*, 2010.
- [20] J.-M. Morel G. Randall R. Grompone von Gioi, J. Jakubowicz. Lsd: A fast line segment detector with a false detection control. *IEEE Trans. on PAMI*, 99, 2008.
- [21] C. C Slama. *Manual of Photogrammetry, 4th edition*. Falls Church, American Society of Photogrammetry, Virginia, 1980.
- [22] Gideon P. Stein. Lens distortion calibration using point correspondences. *CVPR*, 602–608, 1997.
- [23] Roger Y. Tsai. A versatile camera calibration technique for high-accuracy 3d machine vision metrology using off-the-shelf tv cameras and lenses. *IEEE Journal of Robotics and Automation*, Vol. RA-3, 1987.
- [24] J. Weng, P. Cohen, and M. Herniou. Camera calibration with distortion models and accuracy evaluation. *TPAMI*, 14(10):965–980, 1992.
- [25] Z. Zhang. On the epipolar geometry between two images with lens distortion. *Proceedings of the 1996 International Conference on Pattern Recognition*, 7270:407, 1996.
- [26] Z. Zhang. A flexible new technique for camera calibration. *ICCV*, pages 663–673, September 1999.